Effect of topographic correction on forest change detection using spectral trend analysis of Landsat pixel-based composites

Curtis M. Chance[1], Txomin Hermosilla[1], Nicholas C. Coops[1], Michael A. Wulder[2], and Joanne C. White[2]

Affiliations:

[1]Integrated Remote Sensing Studio, Department of Forest Resources Management, University of British Columbia, 2424 Main Mall, Vancouver, BC, V6T 1Z4, Canada
[2]Canadian Forest Service (Pacific Forestry Centre), Natural Resources Canada, 506 West Burnside Road, Victoria, British Columbia, V8Z 1M5, Canada

Corresponding author: curtis.chance@alumni.ubc.ca

Pre-print of published version

Reference:

Chance, C.M., Hermosilla, T., Coops, N.C., Wulder, M.A., and White, J.C. (2016). Effect of topographic correction on forest change detection using spectral trend analysis of Landsat pixel-based composites. International Journal of Applied Earth Observations and Geoinformation. 44, 186-194.

DOI: 10.1016/j.jag.2015.09.003

Abstract

Pixel-based image compositing enables production of large-area surface reflectance images that are largely devoid of clouds, cloud shadows, or haze. Change detection with spectral trend analysis uses a dense time series of images, such as pixel-based composites, to quantify the year, amount, and magnitude of landscape changes. Topographically-related shadows found in mountainous terrain may confound trend-based forest change detection approaches. In this study, we evaluate the impact of topographic correction on trend-based forest change detection outcomes by comparing the amount and location of changes identified on an image composite with and without a topographic correction. Moreover, we evaluated two different approaches to topographic correction that are relevant to pixel-based image composites: the first corrects each pixel according to the day of year (DOY) the pixel was acquired, whilst the second corrects all pixels to a single reference date (August 1st), which was also the target date for generating the pixel-based image composite. Our results indicate that a greater area of change is detected when no topographic correction is applied to the image composite, however, the difference in change area detected between no correction and either the DOY or the August 1st correction is minor and less than 1% (0.54–0.85%). The spatial correspondence of these different approaches is 96.2% for the DOY correction and 97.7% for the August 1st correction. The largest differences between the correction processes occur in valleys (0.71-1.14%), upper slopes (0.71-1.09%), and ridges (0.73-1.09%). While additional tests under different conditions and in other environments are encouraged, our results indicate that topographic correction may not be justified in change detection routines computing spectral trends from pixel-based composites.

1. Introduction

The open release of the Landsat image archive in 2008 (Woodcock et al., 2008) has resulted in an increase in the number of spatial and temporal processing and analytical methods (Banskota et al., 2014) associated with large-area analyses from remotely sensed data (Wulder and Coops, 2014). No longer impeded by per-image costs and further enabled by provision of analysis-ready products that have quality geometric co-regisration and calibrated spectral values, users are increasingly empowered (Hansen and Loveland, 2012; Wulder and Coops, 2014), especially for time series investigations (Kennedy et al., 2010). Multiple images with analogous conditions can be combined to create spatially exhaustive image composites based upon individual pixels (Griffiths et al., 2013; Roy et al., 2010; White et al., 2014) rather than a need for cloud-free scenes, with automated algorithms utilized to remove cloud, shadows, and other atmospheric effects (e.g., Zhu and Woodcock, 2012). Access to dense time series and an exhaustive spatial coverage combined with a level of detail that is informative of human and management activities on terrestrial ecosystems has been afforded by Landsat (Wulder et al., 2008). Change detection, with a particular emphasis on forest change, has been a particularly active research area (e.g., Kennedy et al., 2010; Huang et al., 2010), with opportunities to not only capture stand replacing change, but also to relate more subtle changes including magnitude, duration, and preceding and following land cover conditions (Frazier et al., 2014; Hermosilla et al., 2015).

Currently, analysis-ready Landsat Level 1T (standard terrain correction) products include systematic radiometric and geometric corrections, and include the use of a digital elevation model (DEM) for topographic accuracy (USGS, 2013), noting that there is no standard topographic correction applied for terrain shadows. Topographic correction is an image enhancement used to minimize the impact of shadows or varying illumination caused by terrain (Richter, 1998), the effects of which are not well explored regarding Landsat time series imagery and forest change (Banskota et al., 2014). Pixel-based compositing techniques produce images with a range of pixel acquisition dates, resulting in the possibility of terrain shading differences due to a variation in solar azimuth and zenith. Certain image processing activities can be impacted by differences in surface reflectance values that are not indicative of actual surface condition differences, but rather a manifestation of the physical location (see Tan et al., 2013). Varying terrain shadows throughout the year, as may be the case in a time series based on composites, may disrupt spectral trends, potentially causing errors in change detection results (Banskota et al., 2014). However, studies exploring forest change detection and pixel-based composites have not included topographic corrections (e.g., Griffiths et al., 2013; Hermosilla et al., 2015), and a study that investigated the effects of topographic correction on a

land cover classification of pixel-based composites found only a small increase in classification accuracy (Vanonckelen et al., 2015).

The current capacity for processing of large numbers of images for both large area and dense time series is evident (e.g., Griffiths et al., 2012, 2013; Latifovic and Pouliot, 2014; Hermosilla et al., 2015; Senf et al., 2015) with the resulting composites supporting monitoring and reporting programs (White et al., 2014). To ensure the quality of these outcomes, additional investigation to determine the possible impacts of spectral differences attributable to topography on land cover and change applications is required. Topographic correction routines remain time consuming, require access to adequate digital terrain models, and can be implemented in a variety of ways (e.g., Soenen et al., 2005; Richter et al., 2009), with no consensus on the most appropriate approaches to follow, some of which may be land cover or location dependent. Knowledge of whether or not to include a geometric topographic correction in an image compositing and subsequent analysis workflow is an important consideration for resultant product quality as well as for time and data management. In this research we explore the effects of topographic correction on change detection outcomes using spectral trends computed from Landsat imagery. Specifically, this research focuses on the differences in the quantity of change detected in forested areas as well as the variation in this quantity across different topographic positions when using uncorrected composites, and composites from two different topographic correction approaches, one correcting each pixel considering its actual acquisition day of year (DOY), and the other considering a single date for all pixels.

2. Study area and data

2.1. Study Area

The study area is 56,000 km^2 in area and located in southwest British Columbia, Canada. The location is well-suited to examine the effects of mountainous terrain on spectral trends as it includes both the Coast Mountain Range and the Cascade Mountain Range with an elevation range from 0 m to 3236 m (mean: 1401 m, standard deviation: 544 m), a mean slope of 20°, and various complex terrain features, such as valleys, ridges, and avalanche chutes (Figure 1). This study area includes highly productive temperate rainforests of the coast as well as montane forests further east. The mean annual temperature ranges from approximately 10.2°C in the south to 0°C in the north and -6.1°C in high elevations (Figure 1). The mean annual precipitation ranges from approximately 233 mm in the north to 5883 mm in the north (ClimateBC version 5.10, 2015) (Figure 1).

Approximately 62% of the area is forest dominated by western hemlock (*Tsuga hertophylla*), western red cedar (*Thuja plicata*), lodgepole pine (*Pinus contorta*), and white spruce (*Picea glauca*). Of the forested area, approximately 77% has a canopy closure of greater than 50%. The area is subject to sustainable forest management (including fire suppression) which allows for a range of harvest scenarios. Fires are also common in the eastern part of the study area.

2.2. Data

A digital elevation model (DEM) was available from the British Columbia's Terrain Resource Information Management (TRIM) (2014) dataset which covers the entire province, derived from elevation points and lines. The TRIM DEM is a 25 m product, hence for this study, the TRIM DEM was resampled to a 30 m DEM.

The study area is covered by 12 scenes (path / rows) of the Landsat Worldwide Referencing System (WRS-2). We downloaded all available images with less than 70% cloud cover from the United States Geological Survey archive of Level 1 Terrain-Corrected (L1T) Landsat Thematic Mapper (TM) and Landsat Enhanced Thematic Mapper Plus (ETM+) acquired from August 1st ± 30 days from 1984 to 2012. A total of 1279 candidate images were downloaded for inclusion in the annual best-available-pixel composites. August 1st was selected as the central target acquisition date due a to general correspondence with the growing season for the majority of Canada's terrestrial area (McKenney et al., 2006).

3. Methods

3.1. Methods overview

First, three sets of annual Landsat pixel image composites from 1984 to 2012 were created using: (i) no topographic correction, (ii) a day of year topographic correction (hereafter TC_{DOY}) wherein each pixel in the composites are corrected according to their actual acquisition date, and (iii) an August 1st topographic correction (hereafter TC_{Aug1}) wherein each pixel is corrected as though it were acquired on August 1st. Second, change detection using spectral trend analysis was applied to each of the image composites (following (Hermosilla et al. (2015)), and we compared and contrasted the differences in the change detection results. The methods are outlined in detail below.

3.2. Pre-processing and image compositing

Pixel-based image composites were created from Landsat Thematic Mapper (TM) and Enhanced Thematic Mapper Plus (ETM+) imagery according to the methodology from White et

al. (2014). First, the six optical bands of all images were processed through an atmospheric correction using the Landsat Ecosystem Disturbance Adaptive Processing System (LEDPAS) algorithm (Masek et al., 2006). Second, clouds, shadows, and water were masked using the Function of mask (Fmask) algorithm (Zhu and Woodcock, 2012). Following these steps, each pixel was given separate scores for sensor, acquisition day of year, distance to clouds and cloud shadows, and atmospheric opacity, based on Griffiths et al. (2013). For the sensor score, Landsat 5 scored higher than Landsat 7 due to the Landsat 7 Scan Line Corrector (SLC) error (White et al., 2014). Dates of image acquisition were scored based on the number of days from August 1st (Griffiths et al., 2013; White et al., 2014). There were 1279 candidate images for compositing (i.e., acquired within ± 30 days of August 1st with < 70% cloud cover). For each image in each year between 1984 and 2012, the scores were summed and the best pixel (i.e., with the highest score) in the year was chosen to be written to the annual composites (Griffiths et al., 2013; White et al., 2014). Areas in which there was no suitable pixel to contribute to an annual composite were assigned a "no data" value. Of the 1279 candidate images, pixels from 1202 images were ultimately used to build the annual composites. As the focus of this work is on forested areas, agricultural lands were identified and excluded from our analyses using a mask provided by Agriculture and Agri-Foods Canada (2011 data; ftp://ftp.agr.gc.ca/pub/outgoing/aesb-eos-gg/Crop_Inventory/).

3.3 Topographic correction

We applied the sun-canopy-sensor (SCS) topographic correction (TC) algorithm (Gu and Gillespie, 1998) independently to each band of the original pixel-based composites. The SCS correction was designed specifically for forest environments, with special focus on forests with canopy closure greater than 50%. This correction has been shown to be superior in forested landscapes, since it accounts for the sun angle on the terrain as well as the canopy, making it a geometric correction (Gu and Gillespie, 1998; Soenen et al., 2005). While this method does not correct for atmospheric effects itself, and shading or reflectance from other terrain, it has been used as a benchmark for topographic correction (Fan et al., 2014). As one of our objectives was to explore the effect that a pixel-specific DOY topographic correction would have versus a generic DOY correction, we applied the SCS algorithm using two different approaches: (i) we used the acquisition DOY for each individual pixel to provide a pixel-specific correction (hereafter TC_{DOY}); and (ii) we assumed a single acquisition DOY (August 1st; corresponding to the target DOY for image compositing) for all pixels and applied the correction uniformly across the entire pixel-based composites (hereafter TC_{Aug1}).

The SCS topographic correction was achieved by applying Equation (1) where L_n is the corrected reflectance of a pixel, L is the reflectance of a pixel provided from the imagery, α is the slope of

the terrain from the DEM, Θ is the solar zenith angle, and i is the angle of incidence (Gu and Gillespie, 1998; Soenen et al., 2005).

$$L_n = L * \frac{\cos(\alpha)\ \cos(\theta)}{\cos(i)} \quad (1)$$

For each date the solar zenith angle (Θ) and the angle of incidence (i) were calculated using Equation (2) and Equation (3) respectively.

$$\cos(\theta) = \sin(\varphi) * \sin(\delta) + \cos(\varphi) * \cos(\delta)\cos(h) \quad (2)$$

$$\delta\cos(i) = \cos(\theta) * \cos(\alpha) + \sin(\theta) * \cos(\alpha) * \cos(\arcsin(\frac{-\sin(h)\cos(\delta)}{\cos(\theta)}) - asp) \quad (3)$$

where *asp* is the aspect of the terrain from the DEM, φ is the latitude, h is the hour angle, n is the DOY counted from January 1st, and δ is the declination of the sun computed using Equation (4).

$$\delta = -23.44° * \cos\left(\frac{360°}{365} * (n + 10)\right) \quad (4)$$

The hour angle (h) was -22.5°, based on the time being 90 minutes before solar noon, as most of the Landsat TM images in the study area were acquired at approximately this time. The on-the-ground positon was assumed to be the centre of the study area, (Lat: 50.5°, Long: -120°). The study area was sufficiently small that the solar azimuth changed by maximum of only 3.7° and the solar elevation by 4° across the range during a single date.

3.4. Change detection and proxy compositing

Changes were detected using Landsat time series and spectral trend analysis as presented in Hermosilla et al. (2015). Beyond detecting and describing changes and trends, this method produced annual seamless surface reflectance composites (hereafter referred to as proxy composites). This method contained three major stages: breakpoint detection, contextual analysis, and creation of seamless image composites. Pixel values in pixel series, the temporal vector of a pixel, informed the creation of the composites.

Changes were detected following a bottom-up breakpoint detection algorithm described by Keogh et al. (2001), over pixel series using Normalized Burn Ratio (NBR) values. NBR was used because it has been proven to be and effective and reliable spectral index at detecting forest disturbances (Kennedy et al., 2010). Initially, the pixel series comprised of n values were separated into $n-1$ segments. Then, Root-Mean-Square-Error (RMSE) was calculated to determine the cost of merging pairs of adjacent segments. The pair with the lowest cost was merged. Cost values were then iteratively recalculated for new segments until either the maximum number of segments allowed or the maximum cost of merging allowed are reached. The merging cost was adapted throughout the process to ensure that the algorithm met the maximum segment requirement.

To improve the consistency and the spatial cohesion of the temporally detected changes, a contextual analysis was applied spatially. The reliability of correctly determining the year of a change was ranked, and was inversely related to the number of years of missing data (i.e., pixels labelled as "no data") before, during and after the change event. Thus, detected changes with no or few missing data were considered reliable and subsequently labelled with the change year. Changes with missing observations were considered to have a lower reliability. Low reliability changes that were spatially-adjacent to a high-reliability observation within ± one year were re-labelled with the year of the more reliable change. Additionally, change events that had a size less than the minimum mapping unit (MMU) were removed. The MMU size was 0.5 ha, allowing for a sufficiently fine grain to support a range of information needs, including those of national programs such as the National Forest Inventory and spatial carbon accounting activities (White et al., 2014).

As the final step of the method, pixels labelled as "no data" were infilled with higher-reliability proxy values, using the temporal segments produced in the breakpoint detection process. Completion of this process produced gap-free surface reflectance proxy composites, which we used for analysis. We used the NBR values to characterize the change magnitude, which is the difference between the NBR values before and after the change event, and can fall between 0 for no changes and -2 for major changes.

3.5. Assessment of topographic correction on change detection outcomes

To quantify the effects of topographic correction (TC) on change detection outcomes, we used the non-corrected change detection outcome as a benchmark (hereafter NC). We then calculated the difference between the benchmark and each of the topographically corrected outcomes using Equation (5), and the total number of pixels detected as change each year.

$$\%difference = \frac{(\#\ of\ pixels\ NC) - (\#\ of\ pixels\ TC)}{\#\ of\ pixels\ NC} \quad (5)$$

Assessing the location of the differences of detected changes throughout the different treatments is important in determining the spatial similarity of the changes detected. The spatial correspondences between the TC_{DOY} and NC, and the TC_{Aug1} and NC were quantified using Equation (6).

$$Spatial\ correspondence = \frac{\#\ of\ overlapping\ NC\ and\ TC\ pixels}{Total\ \#\ of\ pixels\ NC} \quad (6)$$

The normalized difference is assessed for the entire forested area, as well as the forested area within different topographic strata, to determine where on the landscape the effects of the topographic corrections are most pronounced. The proportion of area detected as change within each strata is also assessed to determine those areas of the landscape have the greatest impact on the differences between the corrections and non-correction processes. These strata were determined using the topographic position index (TPI) (Weiss, 2001) and the Land Facet Corridor Designer extension in ArcGIS 10.3 by Jenness et al. (2013) (Figure 2). This algorithm stratified the study area into 5 topographic positions (in order of increasing TPI value): valleys, lower slopes, gentle slopes, upper slopes, and ridges. Valleys and lower slopes are areas that have lower elevation than most of their surroundings. Valleys have slopes higher than 12.5 degrees. Gentle slopes are near equal in elevation to their surroundings, and have a slope between 0 and 12.5 degrees. Upper slopes and ridges have elevations higher than most of their surroundings, and ridges have slopes above 12.5 degrees.

Following the forest change hierarchy proposed in Hermosilla et al. (In review), three changes were differentiated, including two types of stand-replacing changes, and non-stand-replacing change. The stand replacing changes were either fire, which results in stand mortality, or harvest, which is the temporary removal of trees for utilization. Non-stand-replacing change types were characterized as low magnitude, punctual, trend anomalies that relate year-on-year ephemeral changes and that did not lead to a change in land cover class (i.e., phenology, insects, water stress). All three types of changes were visually identified and assessed by comparing the topographically corrected and non-topographically corrected outputs.

4. Results

Overall, both the TC_{DOY} and the TC_{Aug1} change detection outcomes had less total area changed than NC outcome (Figure 3). NC produced the largest area detected as change, followed by TC_{Aug1} and TC_{DOY}. For TC_{DOY} correction, there is less area identified as change than for the non-corrected composite in 21 of the 27 analyzed years (Figure 3). For the TC_{Aug1} correction, the correction process detects less area as change in 23 of the 27 years (Figure 3). The area detected as change each year ranges from 10000 ha to 78000 ha (Figure 4). The difference in area detected as change for the DOY correction is less than 1% in both cases, with 0.85%, and 0.54% for the August 1st correction and non-corrected composite, respectively (Table 1). The spatial correspondence with NC, on average across all years, is 96.2% (standard deviation: 1.9%) for the TC_{DOY} and is 97.7% (standard deviation: 1.6%) for the TC_{Aug1} (Table 4).

Stratifying the landscape by topographic position indicates where most of the changes, and differences between the changes detected, occur. Across all three sets of changes, most occur on the ridges and valleys (Table 2) and this pattern is relatively consistent for NC, TC_{DOY}, and TC_{Aug1}. Across the five different topographic positions, the normalized percentage difference between the two corrections and the non-correction is similar, with the August 1st differences being smaller across all five of the strata (Table 3). For both the TC_{DOY} correction and TC_{Aug1}, most of the differences in the amount of change detected occur in valleys, upper slopes, and ridges (Table 3).

The TC_{DOY} and TC_{Aug1} perform more closely both overall (Table 1) and throughout the strata (Table 3) than either of the TC processes do when compared to the NC process. The spatial correspondence between TC_{DOY} and TC_{Aug1} is 97.1 % (standard deviation: 1.1%) (Table 4). Still, TC_{Aug1} detects more change than TC_{DOY} in 20 of 26 years (Figure 4). Most of the differences in the between TC_{DOY} and TC_{Aug1} occur in ridges and valleys (Table 3).

Examples of the effects of topographic correction and non-correction for detecting fire and harvesting events are shown in Figure 5a and 5b respectively. The main differences in effects the topographic correction and non-correction are found in non-stand replacing disturbances which are typically more subtle, and may represent low-magnitude variations on the condition of a given land cover type and do not necessary involve a cover change (Lehmann et al., 2013). The application of topographic correction may lead to poorer detection of the subtle changes caused by non-stand replacing disturbances (see example in Figure 5c). Figure 6 indicates that differences between both the TC_{DOY} and TC_{Aug1} correction, and the NC are subtle changes with a NBR value near 0.

5. Discussion

When undertaking change detection applications, images would ideally be from similar dates across years (often called anniversary dates). Given the satellite revisit cycles, image availability and quality, there has been a tolerance around the anniversary date as a target, not an absolute requirement. With pixel-based composites, in contrast to scene-based change analyses, there is an opportunity for greater variability in dates between years due to the pixel-based compositing approach. That is, a given pixel-series will have a greater potential for variability in DOY as a greater number of images are utilized for populating each annual pixel location (following the compositing rules (see Griffiths et al., 2013; White et al., 2014). End users can control for these differences somewhat by constraining the DOY or applying different rule functions to penalize pixels with DOY further from the target date. Differences in illumination

conditions based upon acquisition data are known to have an impact on pixel reflectance in topographically diverse environments. The degree of the impact will be related to the land cover, slope, and aspect (Teillet et al., 1982); but, will also be limited in the BAP context by the preferential target date and bounded temporal window within which images are eligible for inclusion. The implementation of a topographic correction based on sun-sensor geometry standardized for a single date (August 1st) does not account for the actual date of pixel acquisition, and therefore, one would expect more change area to be detected. Our results indicate this was not the case, however, and the TC_{Aug1} actually performs more similarly to the change detection with NC than the TC_{DOY} does. If the NC process is more true to reality, then this implies that the target date is sufficient as the correction date, and using the more processing intensive TC_{DOY} is not necessary. Nonetheless, as the difference between all the approaches is small, topographic correction is likely not justified due to the overhead it adds to processing, especially for large areas.

The stratification results, as expected, confirm that the greatest differences between the corrected and uncorrected change outputs occur in high slopes (Weiss, 2001), which is anticipated as it is in these areas of the terrain that are most influenced by shadows and as a result is where the algorithm is having the most impact (Soenen et al., 2005). Furthermore, Kumar et al. (1997) found that illumination on slopes greater than 20° differed substantially throughout the year between and within aspects. While our results are not directly comparable to this study, they are consistent in that areas with the greatest slopes (ridges, upper slopes, and valleys) experienced the most differences in change detected, and in Kumar et al. (1997) these areas had the greatest illumination differences. Our study, however, shows much smaller differences in changes detected than the differences in illumination in Kumar et al. (1997), likely due to inherent mechanisms in our methods that reduce the differnces between the corrected and uncorrected BAP composites. The pixels in the BAP composites are from July and August, when the solar azimuth and zenith are near their highest points. While there are differences in illumination at different slopes and aspects during this time (Kumar et al., 1997), in July and August from year-to-year the illumination at a pixel (at which the slope and aspect are constant) may not be enough to cause a detected change in the algorithm. Additionally, using a band ratio such as the NBR can reduce the illumination differences between months, as it is a single value calculated from two bands near-equally affected by illumination. Once again, the small difference at a mean <1% in the amount of detected change area between the corrected and uncorrected BAP composites confirms the limited impact of the topographic correction processes on the overall change detection results.

It is clearly evident that stand replacing disturbances (i.e., fire, harvesting) are appropriately detected whether or not a topographic correction is applied. Indeed, our change detection

process (Hermosilla et al., 2015) is designed to be robust to variation in spectral response, so unless illumination conditions related to topography are for some reason markedly different from one year to the next, the process will be able to detect the change. Once again, this variation is constrained by the limited date range used for the compositing. It is the more subtle changes, characterized by low variations in the spectral magnitude, where the differences may occur. Stand-replacing changes have differences in NBR (i.e. change magnitude variation) of -0.5 or smaller. Most of the subtle changes not detected by the topographic corrected routines exhibit values close to 0 (Figure 6), which indicates that the non-stand-replacing changes are slight and likely related to variations in vegetation condition due to sporadic (e.g., defoliation, diseases), or more cyclical events driven by hydrological and/or weather regimes, such as phenological variations, stressed vegetation, or desiccation processes (Hermosilla et al., 2015). Future research could explore the effects of topographic correction on detecting these change types, especially non-stand-replacing changes, in greater detail.

The DEM can introduce noise in topographic correction (Huang et al., 2008; Nichol and Hang, 2008) via sub-pixel variation (Nichol and Hang, 2008; Richter, 1998), and the interpolation method during its creation (Nichol and Hang, 2008). Although not explicit in the results of this study, both the TC_{DOY} and TC_{Aug1} may introduce noise. In our case, the DEM produced artifacts predicting shading on the corrected BAP composites where none is apparent on the uncorrected composites. These artifacts follow terrain contours introducing some undulating lines (Figure 5a and c) in the topographically corrected reflectance values. The change detection process minimizes the effect of these artifacts through the removal of groups of pixels smaller than 0.5 ha, the MMU. Also, since the DEM effects are similar for each year, especially for the TC_{Aug1}, these small shaded areas may have a minimal effect on the differences observed.

In addition to these DEM effects, the SCS correction may overcorrect in steep sloped areas (Soenen et al., 2005). Considering these implications, and the reality that the SCS correction is designed to function best in forests with > 50% canopy closure (Gu and Gillespie, 1998; Soenen et al., 2005), the topographic correction process brings with it numerous decision factors and processing considerations. This is especially true for pixel-based composites, due to the larger areas that they may cover, as well as the fact that pixels in pixel-based composites are acquired from a range of dates. For these reasons and the small differences between the TC_{DOY}, TC_{Aug1}, and NC processes, the processing and time costs of the terrain-based geometric topographic correction process may not be justified for change detection applications using pixel-based composites.

6. Conclusions

In this research we analyze the effect of topographic correction on forest change predicted from time series of Landsat pixel-based image composites. To do this, we topographically corrected the image composites using the sun-canopy-sensor correction algorithm. The spectral trends of the composites were analyzed to detect non-stand-replacing changes. We assessed the effects of the algorithm using two different correction dates: August 1st, in which each pixel was corrected as though it had been acquired on that date, and a day of year correction, in which each pixel was corrected based on its actual date of acquisition. We assessed the impact of these topographic corrections by comparing change detection outputs against change detection outputs generated when no topographic correction was applied to the image composites. Our results indicate that topographic correction does not cause a substantial difference in the forest change detection results with a 0.54–0.85% difference in changes detected compared to the non-corrected images. Stand replacing disturbances such as fire and harvest are detected well by both; however, in cases of non-stand replacing disturbances, - where there are subtle, low magnitude changes on the landscape, - the addition of a topographic correction in the change detection workflow negatively impacted the detection of these changes. Our results indicate that a terrain-based geometric topographic correction may not be justified in change detection routines computing spectral trends from pixel-based composites. Further research may explore the effects of other correction methods on similar change detection processes.

Acknowledgements

Geordie Hobart of the Canadian Forest Service is acknowledged for preparation of the annual pixel-based composites used in this research. This research was undertaken as part of the "National Terrestrial Ecosystem Monitoring System (NTEMS): Timely and detailed national cross-sector monitoring for Canada" project jointly funded by the Canadian Space Agency (CSA) Government Related Initiatives Program (GRIP) and the Canadian Forest Service (CFS) of Natural Resources Canada. Additional support was provided by an NSERC Discovery grant to Coops. We appreciate the time, effort, and insight offered by the journal editors and reviewers.

References

Banskota, A., Kayastha, N., Falkowski, M.J., Wulder, M. a., Froese, R.E., White, J.C., 2014. Forest Monitoring Using Landsat Time Series Data: A Review. Can. J. Remote Sens. 40, 362–384. doi:10.1080/07038992.2014.987376

Fan, Y., Koukal, T., Weisberg, P.J., 2014. A sun-crown-sensor model and adapted C-correction logic for topographic correction of high resolution forest imagery. ISPRS J. Photogramm. Remote Sens. 96, 94–105. doi:10.1016/j.isprsjprs.2014.07.005

Frazier, R.J., Coops, N.C., Wulder, M. a, Kennedy, R., 2014. Characterization of aboveground biomass in an unmanaged boreal forest using Landsat temporal segmentation metrics. Isprs J. Photogramm. Remote Sens. 92, 137–146. doi:10.1016/j.isprsjprs.2014.03.003

Griffiths, P., Kuemmerle, T., Baumann, M., Radeloff, V.C., Abrudan, I. V., Lieskovsky, J., Munteanu, C., Ostapowicz, K., Hostert, P., 2013. Forest disturbances, forest recovery, and changes in forest types across the Carpathian ecoregion from 1985 to 2010 based on Landsat image composites. Remote Sens. Environ. doi:10.1016/j.rse.2013.04.022

Griffiths, P., Kuemmerle, T., Kennedy, R.E., Abrudan, I. V., Knorn, J., Hostert, P., 2012. Using annual time-series of Landsat images to assess the effects of forest restitution in post-socialist Romania. Remote Sens. Environ. 118, 199–214. doi:10.1016/j.rse.2011.11.006

Griffiths, P., van der Linden, S., Kuemmerle, T., Hostert, P., 2013. A Pixel-Based Landsat Compositing Algorithm for Large Area Land Cover Mapping. Sel. Top. Appl. Earth Obs. Remote Sensing, IEEE J. 6, 2088–2101. doi:10.1109/JSTARS.2012.2228167

Gu, D., Gillespie, A., 1998. Topographic normalization of Landsat TM images of forest based on subpixel sun-canopy-sensor. Remote Sens. Environ. 64, 166–175.

Hansen, M.C., Loveland, T.R., 2012. A review of large area monitoring of land cover change using Landsat data. Remote Sens. Environ. 122, 66–74. doi:10.1016/j.rse.2011.08.024

Hermosilla, T., Wulder, M.A., White, J.C., Coops, N.C., Hobart, G.W., 2015. An integrated Landsat time series protocol for change detection and generation of annual gap-free surface reflectance composites. Remote Sens. Environ. 158, 220–234. doi:10.1016/j.rse.2014.11.005

Hermosilla, T., Wulder, M.A., White, J.C., Coops, N.C., Hobart, G.W., (In review). Regional detection, characterization, and attribution of annual forest change from 1984 to 2012 using Landsat-derived time-series metrics. Remote Sensing of Environment (minor revision submitted on August 11 2015).

Huang, C., Goward, S.N., Masek, J.G., Thomas, N., Zhu, Z., Vogelmann, J.E., 2010. An automated approach for reconstructing recent forest disturbance history using dense Landsat time series stacks. Remote Sens. Environ. 114, 183–198. doi:10.1016/j.rse.2009.08.017

Huang, H., Gong, P., Clinton, N., Hui, F., 2008. Reduction of atmospheric and topographic effect on Landsat TM data for forest classification. Int. J. Remote Sens. 29, 5623–5642. doi:10.1080/01431160802082148

Jenness, J., Brost, B., Beier, P., 2013. Land Facet Corridor Designer: Extension for ArcGIS.

Kennedy, R.E., Yang, Z., Cohen, W.B., 2010. Detecting trends in forest disturbance and recovery using yearly Landsat time series : 1 . LandTrendr — Temporal segmentation algorithms. Remote Sens. Environ. 114, 2897–2910. doi:10.1016/j.rse.2010.07.008

Keogh, E., Chu, S., Hart, D., Pazzani, M., 2001. An online algorithm for segmenting time series. Data Mining, 2001. ICDM … 289–296. doi:10.1109/ICDM.2001.989531

Kumar, L., Skidmore, A.K., Knowles, E., 1997. Modelling topographic variation in solar radiation in a GIS environment. Int. J. Geogr. Inf. Sci. 11, 475–497. doi:10.1080/136588197242266

Latifovic, R., Pouliot, D., 2014. Monitoring Cumulative Long-Term Vegetation Changes Over the Athabasca Oil Sands Region. IEEE J. Sel. Top. Appl. Earth Obs. Remote Sens. 7, 1–13. doi:10.1109/JSTARS.2014.2321058

Lehmann, E.A., Wallace, J.F., Caccetta, P.A., Furby, S.L., Zdunic, K., 2013. Forest cover trends from time series Landsat data for the Australian continent. Int. J. Appl. Earth Obs. Geoinf. 21, 453–462. doi:10.1016/j.jag.2012.06.005

Masek, J.G., Vermote, E.F., Saleous, N.E., Wolfe, R., Hall, F.G., Huemmrich, K.F., Gao, F., Kutler, J., Lim, T.K., 2006. A Landsat surface reflectance dataset for North America, 1990-2000. Geosci. Remote Sens. Lett. IEEE 3, 68–72.

McKenney, D., Pedlar, J., Papadopol, P., Hutchinson, M., 2006. The development of 1901–2000 historical monthly climate models for Canada and the United States. Agric. For. … 138, 69–81. doi:10.1016/j.agrformet.2006.03.012

Nichol, J., Hang, L.K., 2008. The influence of DEM accuracy, on topographic correction of Ikonos satellite images. Photogramm. Eng. Remote Sensing 74, 47–53.

Richter, R., 1998. Correction of satellite imagery over mountainous terrain. Appl. Opt. 37, 4004–15.

Richter, R., Kellenberger, T., Kaufmann, H., 2009. Comparison of topographic correction methods. Remote Sens. 1, 184–196. doi:10.3390/rs1030184

Roy, D.P., Ju, J., Kline, K., Scaramuzza, P.L., Kovalskyy, V., Hansen, M., Loveland, T.R., Vermote, E., Zhang, C., 2010. Web-enabled Landsat Data (WELD): Landsat ETM+ composited mosaics of the conterminous United States. Remote Sens. Environ. 114, 35–49. doi:10.1016/j.rse.2009.08.011

Senf, C., Leitão, P.J., Pflugmacher, D., van der Linden, S., Hostert, P., 2015. Mapping land cover in complex Mediterranean landscapes using Landsat: Improved classification accuracies from integrating multi-seasonal and synthetic imagery. Remote Sens. Environ. 156, 527–536. doi:10.1016/j.rse.2014.10.018

Soenen, S.A., Peddle, D., Coburn, C.A., 2005. SCS+C: A modified sun-canopy-sensor topographic correction in forested terrain. IEEE Trans. Geosci. Remote Sens. 43, 2148–2159.

Tan, B., Masek, J.G., Wolfe, R., Gao, F., Huang, C., Vermote, E.F., Sexton, J.O., Ederer, G., 2013. Improved forest change detection with terrain illumination corrected Landsat images. Remote Sens. Environ. 136, 469–483.

Teillet, P.M., Guindon, B., Goodenough, D.G., 1982. On the slope-aspect correction of multispectral scanner data. Can. J. Remote Sens. 8, 84–106.

TRIM, B., 2014. British Columbia Terrain Resource Information Mapping (TRIM) Digital Map Products. B.C. Ministry of Sustainable Resource Management, Base Mapping and Geomatics Services Branch. [WWW Document]. URL http://geobc.gov.bc.ca/base-mapping/atlas/trim/ (accessed 5.30.14).

USGS, 2013. Product guide: Landsat climate data record (CDR). Surface reflectance.

Vanonckelen, S., Lhermitte, S., Rompaey, A. Van, 2015. International Journal of Applied Earth Observation and Geoinformation The effect of atmospheric and topographic correction on pixel-based image composites : Improved forest cover detection in mountain environments. Int. J. Appl. Earth Obs. Geoinf. 35, 320–328. doi:10.1016/j.jag.2014.10.006

Weiss, A.D., 2001. Topographic position and landforms analysis. Poster Present. ESRI User Conf. San Diego, CA.

White, J.C., Wulder, M. a., Hobart, G.W., Luther, J.E., Hermosilla, T., Griffiths, P., Coops, N.C., Hall, R.J., Hostert, P., Dyk, A., Guindon, L., 2014. Pixel-based image compositing for large-area dense time series applications and science. Can. J. Remote Sens. 40, 192–212. doi:10.1080/07038992.2014.945827

Woodcock, C.E., Allen, R., Anderson, M., Belward, A., Bindschadler, R., Cohen, W., Gao, F., Goward, S.N., Helder, D., Helmer, E., Nemani, R., Oreopoulos, L., Schott, J., Thenkabail, P.S., Vermote, E.F., Vogelmann, J., Wulder, W.A., R., W., 2008. Free access to Landsat Imagery. Science (80-.). 320, 5879.

Wulder, M.A., Coops, N.C., 2014. Make Earth observations open access. Nature 513 (7516), 30–31.

Wulder, M.A., White, J.C., Goward, S.N., Masek, J.G., Irons, J.R., Herold, M., Woodcock, C.E., 2008. Landsat continuity: Issues and opportunities for land cover monitoring. Remote Sens. Environ. 112, 955–969. doi:10.1016/j.rse.2007.07.004

Zhu, Z., Woodcock, C.E., 2012. Object-based cloud and cloud shadow detection in Landsat imagery. Remote Sens. Environ. 118, 83–94. doi:10.1016/j.rse.2011.10.028

Table 1. Mean and coefficient of variation (CV) of the absolute value of the percent difference between the number of pixels detected as change in the correction and the no correction (NC) for the two correction treatments, the day of year (TC_{DOY}) correction and the August 1st correction (TC_{Aug1}), and between the two correction treatments. Equation ((5)) was used to calculate the percent difference for the two correction treatments.

		TC_{DOY}, NC	TC_{Aug1}, NC	TC_{DOY}, TC_{Aug1}
Difference of areas detected as change	Mean	0.85%	0.54%	0.36%
	CV	1.08%	0.98%	2.05%

Table 2. Proportion of changes detected, for all years, for each topographic position for the three change detection process: a day of year (TC_{DOY}) topographic correction, an August 1st topographic correction (TC_{Aug1}), and no topographic correction (NC).

Topographic Position	TC_{DOY}	TC_{Aug1}	NC
Valley	36.26%	36.26%	36.40%
Lower slope	8.89%	8.83%	8.89%
Gentle slope	12.26%	12.40%	12.21%
Upper slope	6.17%	6.17%	6.17%
Ridge	36.42%	36.45%	36.36%

Table 3. Mean of the absolute value of the percent difference between the number of pixels detected as change in the correction and the non-correction for the two correction treatments, the day of year (TC_{DOY}) correction and the August 1st correction (TC_{Aug1}) for each topographic position. Equation ((5)) was used to calculate the percent difference for the two correction treatments.

Topographic position	TC_{DOY}, NC	TC_{Aug1}, NC	TC_{DOY}, TC_{Aug1}
Valley	1.14%	0.70%	0.39%
Lower slope	0.69%	0.50%	0.24%
Gentle slope	0.45%	0.26%	0.13%
Upper slope	1.09%	0.71%	0.21%
Ridge	1.09%	0.73%	0.40%

Table 4. Spatial correspondence in percent of pixels of detected changes overlapping, as determined by Equation 6, for the no correction (NC) process, the day of year topographic correction (TC_{DOY}), and the August 1st topographic correction (TC_{Aug1}).

	NC	TC_{DOY}	TC_{Aug1}
NC	100.0%	96.2%	97.7%
TC_{DOY}	-	100.0%	97.1%
TC_{Aug1}	-	-	100.0%

Figure 1. Location of the study area within North America and British Columbia, a) an image composite of Landsat imagery from 2012 displaying the band combination 5, 4, 3, b) the digital terrain model with red representing high elevations and dark green representing low elevations, c) the mean annual temperature across the study area, and d) the mean annual precipitation across the study area.

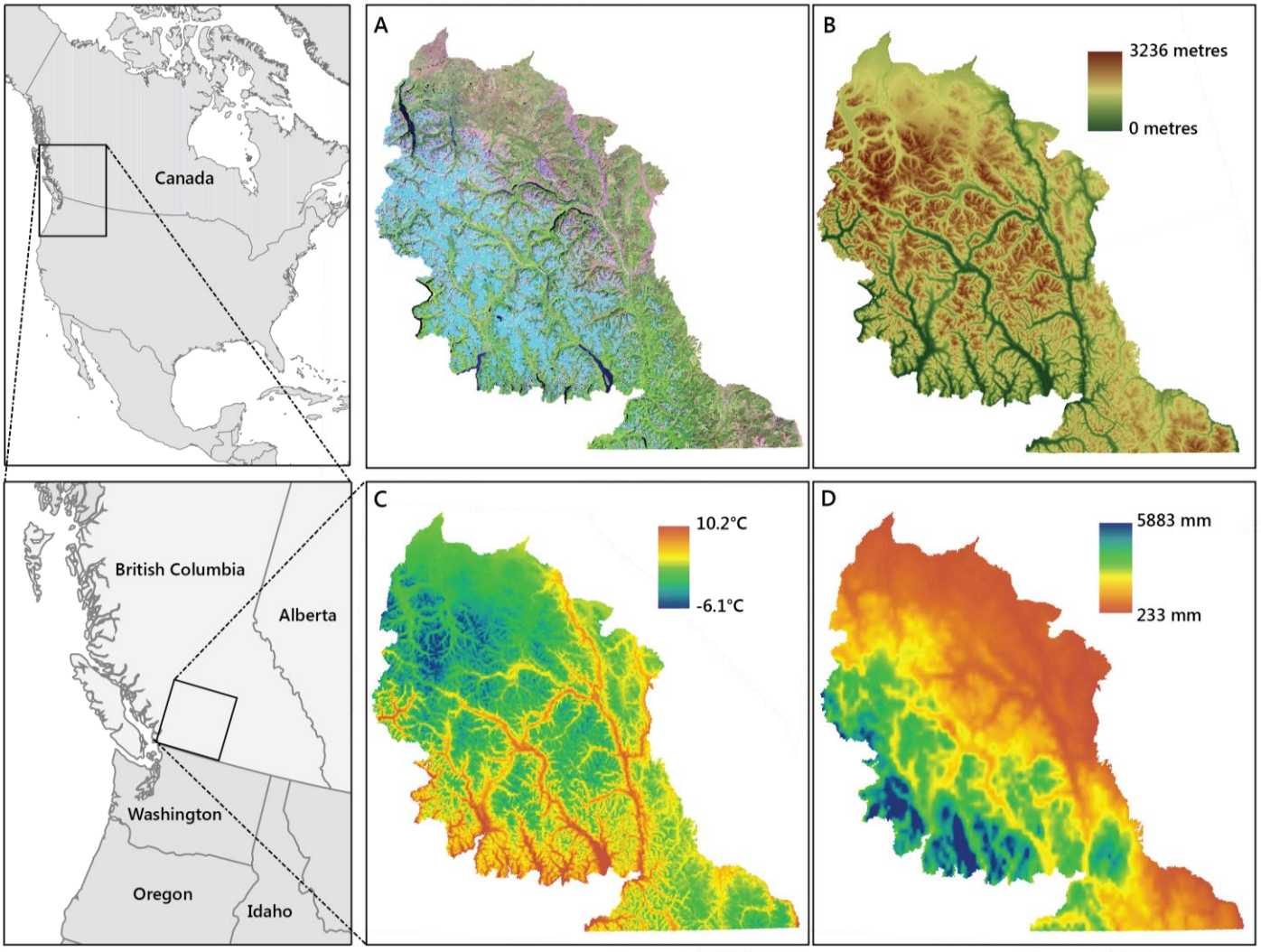

Figure 2. Representation of strata used in this study, as determined by the topographic position index (TPI).

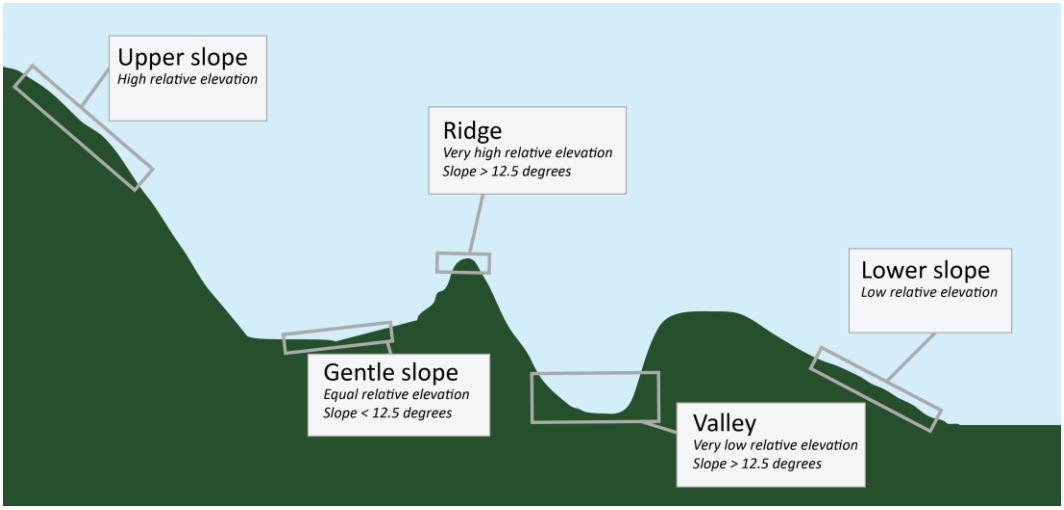

Figure 3. Percent difference of pixels classified as change between the day of year (TC_{DOY}) correction and the non-correction (NC), and the August 1st correction (TC_{Aug1}) and the non-correction (NC), as calculated from Equation (5).

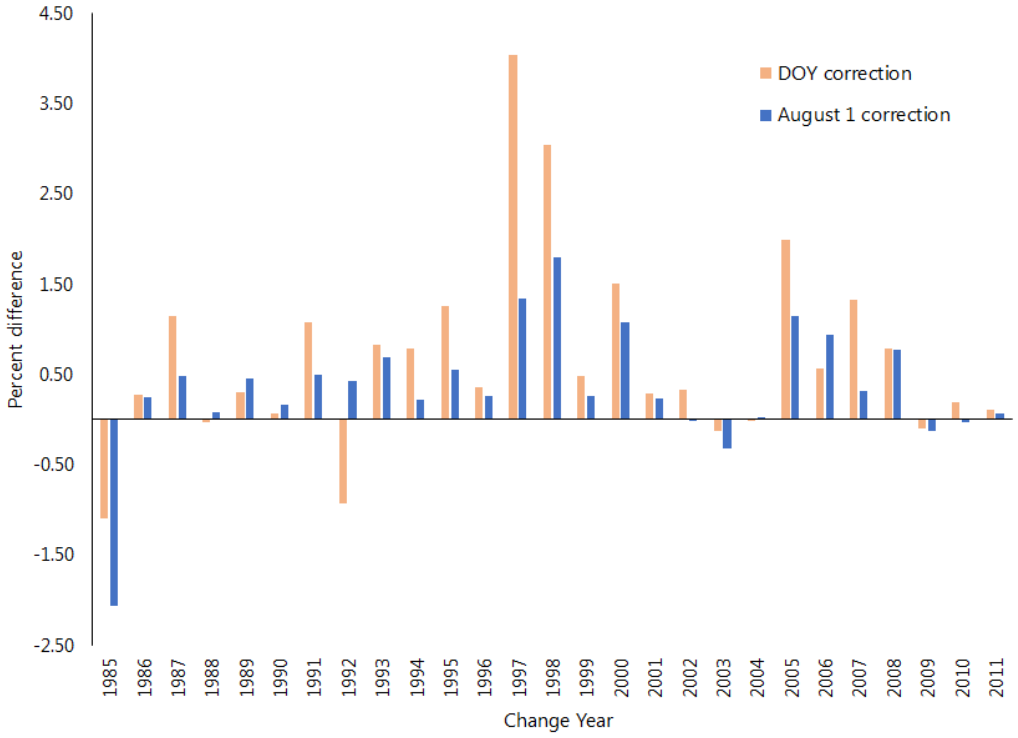

Figure 4. Area detected as change each year for the non-correction and the day of year (DOY) correction and August 1st correction.

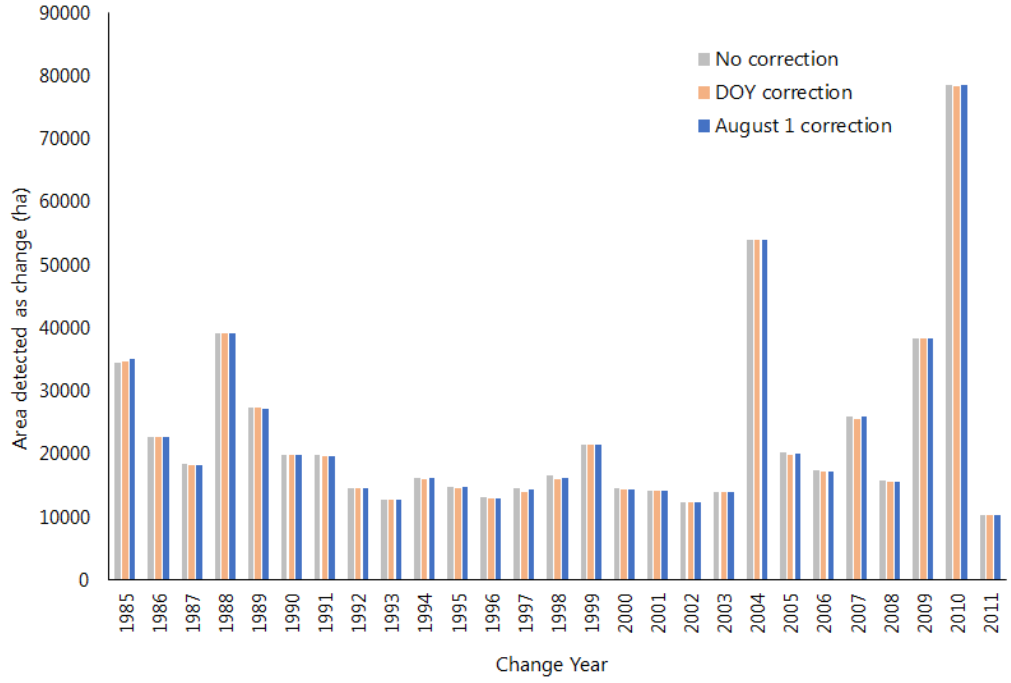

Figure 5. BAP proxy 5,4,3 composites showing the difference in (a) harvest-caused changes, (b) fire-caused changes, and (c) non-stand-replacing changes detected between day of year (DOY) topographically corrected images and uncorrected images for the study area.

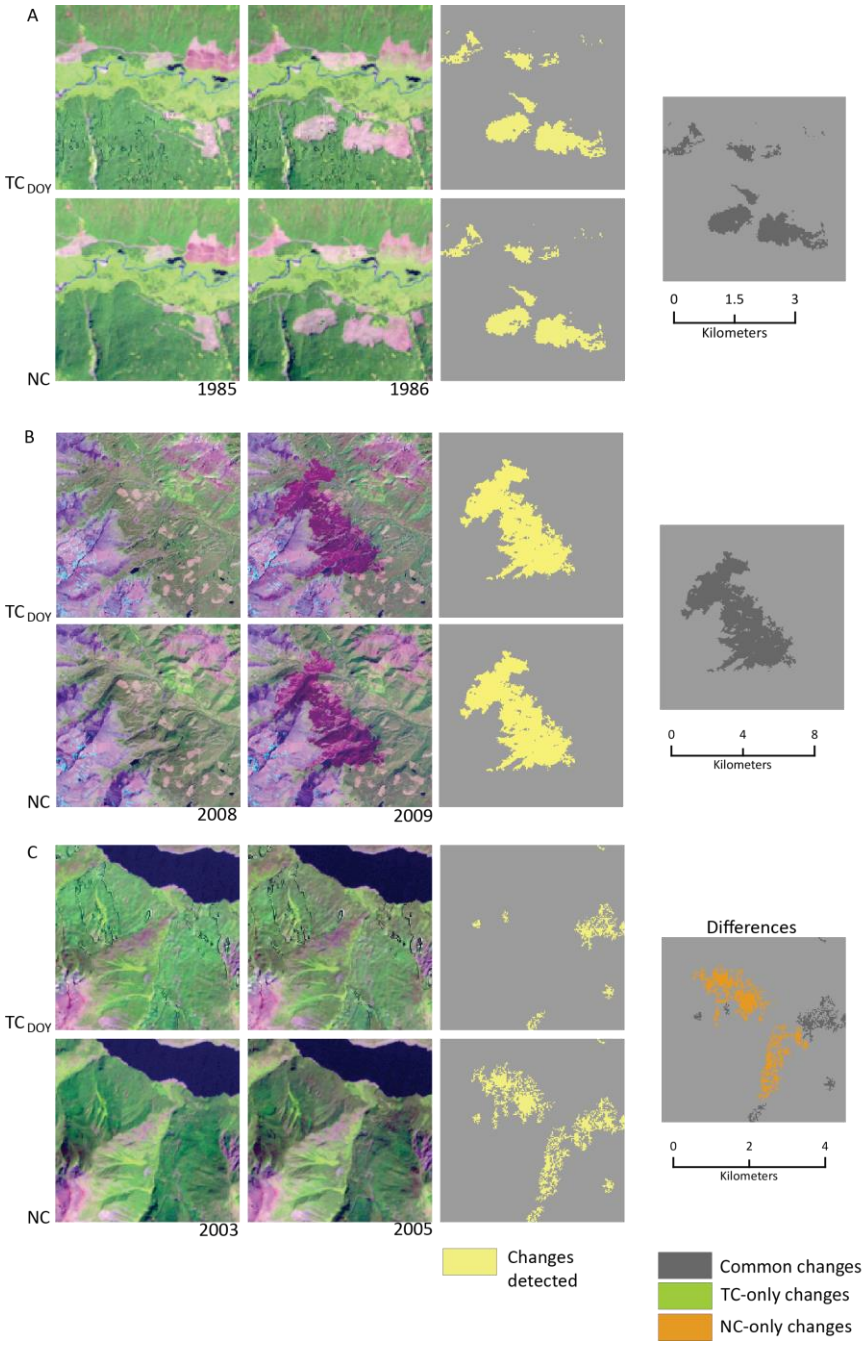

Figure 6. All area detected as change in the non-correction process, that not detected in the day of year (DOY) correction and August 1st correction, and the normalized burn ratio (NBR) value associated with the changes. Although values of this metric vary from -2 to 0 (corresponding to the maximum possible difference between two NBR values), x-axis shows from -1.3 to 0 for displaying purposes.